

## Supporting Information

# Water-repellent TiO<sub>2</sub>-Organic dye-based Air Filters for Efficient Visible-light-activated Photochemical Inactivation against Bioaerosols

*Ki Joon Heo<sup>a,†</sup>, Sang Bin Jeong<sup>b,c,†</sup>, Juhun Shin<sup>d</sup>, Gi Byoung Hwang<sup>d</sup>, Hyun Sik Ko<sup>e</sup>, Yeonsang Kim<sup>a</sup>, Dong Yun Choi<sup>f,\*</sup>, and Jae Hee Jung<sup>e,\*</sup>*

<sup>a</sup> Advanced Textile R&D Department, Korea Institute of Industrial Technology (KITECH), Ansan 15588, Republic of Korea

<sup>b</sup> Graduate School of Energy and Environment, Korea University, Seoul 02841, Republic of Korea

<sup>c</sup> Center for Environment, Health, and Welfare Research, Korea Institute of Science and Technology, Seoul 02792, Republic of Korea

<sup>d</sup> Materials Chemistry Research Centre, Department of Chemistry, University College London, London, WC1H 0AJ, United Kingdom

<sup>e</sup> Aerosol and Particle Technology Laboratory, Department of Mechanical Engineering, Sejong University, Seoul 05006, Republic of Korea

<sup>f</sup> Biomedical Manufacturing Technology Center, KITECH, Yeongcheon, 38822, Republic of Korea

<sup>†</sup> These authors contributed equally to this work.

\* Correspondence should be addressed to

: [dychoi311@kitech.re.kr](mailto:dychoi311@kitech.re.kr), Tel.: 82-54-339-0523

: [jaehee@sejong.ac.kr](mailto:jaehee@sejong.ac.kr), Tel.: 82-2-3408-1849

## MATERIALS AND METHODS

**Preparation of visible-light-activated (VLA) nanoparticles** A solution was prepared by dispersing 1.0 g 1H,1H,2H,2H-perfluorooctyltriethoxysilane [PFOTES; C<sub>8</sub>F<sub>13</sub>H<sub>4</sub>Si(OCH<sub>2</sub>CH<sub>3</sub>)<sub>3</sub>; Sigma-Aldrich, St. Louis, MO, USA] in 99.0 g pure ethanol, with agitation for 10 min. Then, 4.0 g titanium dioxide (TiO<sub>2</sub>) nanoparticles (NPs) (99.5%, Sigma-Aldrich) and 40 mg crystal violet (CV; C<sub>25</sub>N<sub>3</sub>H<sub>30</sub>Cl; Sigma-Aldrich) were mixed with 40 mL of the PFOTES solution with steady agitation. The mixture was vortexed and sonicated for 5 min.

**Characterization of VLA nanoparticles** A UV-Vis spectrometer (Lambda 25, PerkinElmer Inc., Shelton, CT, USA) with a wavelength detection range of 190–1100 nm and wavelength accuracy of ± 0.1 nm was used. Characterization of ultraviolet and visible absorption spectra was conducted using an intact glass (control) and NPs fixed in glass at 380–700 nm.

X-ray photoelectron spectroscopy (XPS) was used to determine the band offset of CV (C<sub>25</sub>N<sub>3</sub>H<sub>30</sub>Cl) and TiO<sub>2</sub> using the method proposed by Bernède et al. Core levels of N1s and Ti2p, homo band maximum (HBM) for CV, and valance band maximum (VBM) for TiO<sub>2</sub> were measured. Band alignment and energy offset were determined by the equation below:

$$\Delta E_{\text{HVBM}} = (E_{\text{N1s}}^{\text{CV}} - E_{\text{HBM}}^{\text{CV}}) - (E_{\text{Ti2p}}^{\text{TiO}_2} - E_{\text{VBM}}^{\text{TiO}_2}) - \Delta E_{\text{CL}} \quad (1)$$

where  $\Delta E_{\text{HVBM}}$  is the offset between CV HBM and TiO<sub>2</sub> VBM,  $\Delta E_{\text{CL}}$  is the energy difference between  $E_{\text{N1s}}^{\text{CV}}$  and  $E_{\text{Ti2p}}^{\text{TiO}_2}$  levels at the interface of CV and TiO<sub>2</sub>,  $E_{\text{HBM}}^{\text{CV}}$  and  $E_{\text{VBM}}^{\text{TiO}_2}$  are the energy of CV HBM and TiO<sub>2</sub> VBM, respectively, and  $\Delta E_{\text{LBM}}$  is the energy difference between the CV lumo band maximum (LBM) and the TiO<sub>2</sub> conduction band maximum (CBM) level. In addition, Shirley background and Gaussian–Lorentzian profiles were used to find the positions of the peaks in the XPS spectra.

**Preparation of the VLA antimicrobial filter** To aerosolize the VLA NPs, 30 mL TiO<sub>2</sub>@PFOTES-CV solution diluted with pure ethanol to 2% (w/w) was loaded into a

six-jet Collison Nebulizer (BGI Inc., Waltham, MA, USA) (Fig. S2a). An airflow of 5 L/min, which was filtered through a high-efficiency particulate air filter, was supplied to the nebulizer using a mass flow controller (GMC1200, Atovac, Yongin, Korea) at a pressure of 1 psig. The aerosolized TiO<sub>2</sub>@PFOTES-CV NPs were passed through a carbon diffusion dryer to eliminate any remaining ethanol and continuously deposited onto a polyurethane fiber filter, which is the filter typically used in conventional facepieces. The particles were deposited on the pristine filters, which were round with a diameter of 1 inch, for 1, 3, 5, and 7 min. The particle size distribution and concentration of the aerosolized TiO<sub>2</sub>@PFOTES-CV NPs were evaluated using a scanning mobility particle sizer (model 3080, TSI Inc., Shoreview, MN, USA) through an aerosol neutralizer (4530; HCT, Incheon, Korea). Following aerosol deposition, the deposits on the filters were quantified by weighing the filters before and after deposition using a microbalance (Mettler MT5; Mettler-Toledo International, Seoul, Korea). The morphology of the test filter was investigated using scanning electron microscopy (Hitachi, Tokyo, Japan).

**Preparation of bacterial suspensions** Filtration and VLA antimicrobial performance were evaluated using four bacterial strains obtained from the Korean Collection for Type Cultures (KCTC): Gram-positive *S. epidermidis* (KCTC 1917) and *B. subtilis* (KCTC 2189) and Gram-negative *E. coli* (KCTC 1039) and *E. aerogenes* (KCTC 2190). All bacteria were incubated on nutrient broth (beef extract 0.3% and peptone 0.5%; Becton Dickinson, Franklin Lakes, NJ, USA) at 30°C (*B. subtilis*) or 37°C (*S. epidermidis*, *E. coli*, and *E. aerogenes*) at 200 rpm. When the bacterial medium reached an optical density of ~0.6 at 600 nm, the bacteria were harvested by centrifugation (4000 × g for 15 min) and washed three times using deionized water. Then, 1 mL bacterial suspension was mixed with 19 mL deionized water and loaded into the Collison nebulizer for aerosolization.

**Filtration test** Figure S12 presents a schematic representation of the apparatus used to evaluate the filtration performance of the TiO<sub>2</sub>@PFOTES-CV filter. The bacterial droplets were aerosolized using an airflow of 5 L/min at a pressure of 1 psig, and the moisture was removed by passing through a diffusion dryer (silica gel; Kanto Chemical, Tokyo, Japan). Bacterial aerosols are widely used as a representative of bioaerosols,

including a standard face mask testing method.<sup>1</sup> To reduce any effect of charge, the bacterial aerosols were passed through a soft X-ray neutralizer before introducing the filter holder. The size distribution and concentration of bacterial aerosols were measured at the inlet and outlet of the filter holder using an aerodynamic particle sizer (APS; model 3321, TSI Inc.), and the filtration efficiencies were calculated as follows:

$$\eta = 1 - (C_{\text{outlet}}/C_{\text{inlet}}) \quad (2)$$

where  $C_{\text{outlet}}$  and  $C_{\text{inlet}}$  are the particle concentrations (particles/cm<sup>3</sup><sub>air</sub>) at the outlet and inlet of the filter holder, respectively. The pressure drop of the test filters was measured using a micro-manometer (FC012; Furness Control, Ltd., Bexhill, UK).

**Visible light-activated antimicrobial effects against bioaerosols** Bacterial aerosols were deposited continuously onto the TiO<sub>2</sub>@PFOTES-CV filter for 10 min in all experiments. Then, the test filters with bacteria particles were placed on a moisture box to maintain humidity and covered with a sterile glass slide to maintain proper contact between the surface of the test filter and the bacteria (Fig. S4). Subsequently, the filters were exposed to visible light using a 28 W white fluorescent lamp (GE Lighting, East Cleveland, OH, USA), and another set of samples was placed in a dark chamber for various periods of time. The optical power (mW) of the fluorescent lamp was measured using a power meter (PM200; Thorlabs Inc., Newton, NJ, USA) and a photodiode power sensor (S120C; Thorlabs Inc.). Following light exposure, the samples were placed in 15 mL ( $V_{\text{extraction,filter}}$ ) phosphate-buffered saline (PBS) containing 0.01% Tween 80 and vortexed for 5 min to transfer the bacterial particles from the filter to the PBS solution.

The resulting bacterial suspension from the test filters was serially diluted onto a nutrient agar plate (0.3% beef extract and 0.5% peptone; Becton Dickinson) and incubated at 30°C (*B. subtilis*) or 37°C (*S. epidermidis*, *E. coli*, and *E. aerogenes*) for 24 h. Bacterial colony forming units (CFUs) were counted after incubation, and the antimicrobial efficiency was calculated as follows:

$$C_o = \text{CFU}_{\text{control}}/\text{BC}_{\text{control}} \quad (3)$$

$$C = \text{CFU}_{\text{TPCV}}/\text{BC}_{\text{TPCV}} \quad (4)$$

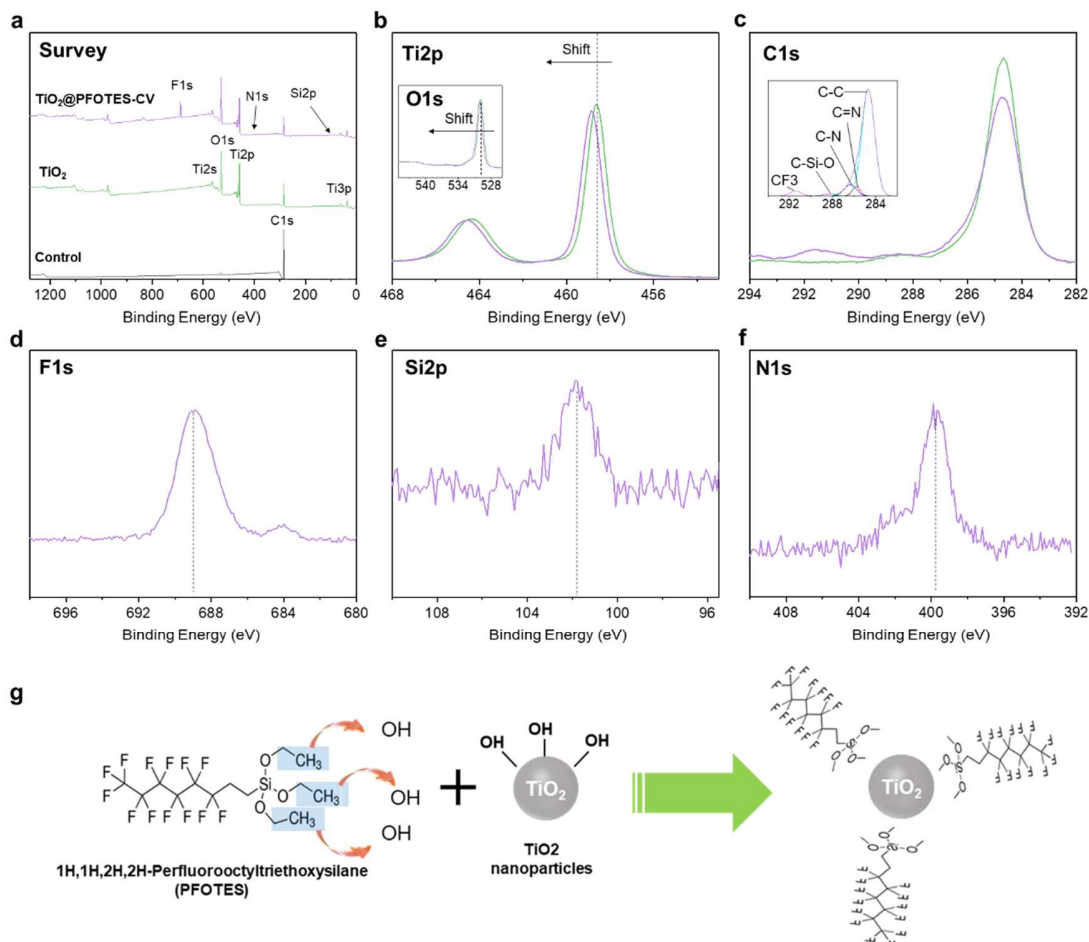
$$BC_{\text{control or TPCV}} = \frac{C_{\text{inlet}} \cdot Q_{\text{sampling}} \cdot \eta \cdot \xi_{\text{extraction}}}{V_{\text{extraction,filter}}} \quad (5)$$

where  $C_o$  and  $C$  are the active proportions of bacteria from the control and TiO<sub>2</sub>@PFOTES-CV filter, respectively; BC is the total bacterial concentration (particles/mL) in the extracted suspension on the agar plate;  $C_{\text{inlet}}$  is the concentration of bacterial aerosols from the nebulizer;  $Q_{\text{sampling}}$  is the total sampling air volume; and  $\xi_{\text{extraction}}$  is the physical extraction of bacteria from each filter, defined as the ratio of the number of particles transferred from the filter into the extraction liquid to the number of particles removed from airflow using the filter. It was assumed that the  $\xi_{\text{extraction}}$  values were identical among all tested filters.

**Classification of reactive oxygen species (ROS)** The mechanism of VLA antimicrobial effects was evaluated using scavengers or quenchers of ROS. Catalase, *L*-histidine, mannitol, and superoxide dismutase were purchased from Sigma-Aldrich. Catalase was used at a concentration of 6–14 units/mL in bacterial suspension to remove hydrogen peroxide, since the concentration of catalase was 2,000–5,000 units/mg protein. *L*-histidine was used at a concentration of 2 mM in bacterial suspension as a singlet oxygen (<sup>1</sup>O<sub>2</sub>) quencher. Mannitol was used at a concentration of 82 mM in bacterial suspensions to eliminate hydroxyl radicals (•OH). Superoxide dismutase was used at a concentration of 20 units/mL in bacterial suspensions to remove superoxide radicals (O<sub>2</sub><sup>•-</sup>). The *S. epidermidis* bacterial suspension (~1.8 × 10<sup>4</sup> CFU/mL) including ROS scavenger or quencher was maintained in 3 mL glass bowls. TiO<sub>2</sub>@PFOTES-CV filters were submerged in each bacterial suspension, and visible light was irradiated at an optical power of 6.9 mW/cm<sup>2</sup> for 4 h. The resulting bacterial suspension from each test was serially diluted onto a nutrient agar plate and incubated at 37°C for 24 h. The bacterial colony concentration (CFU/mL) was determined for classification of ROS.

**Stability tests of the antimicrobial air filters** The adhesion stability test of deposited TiO<sub>2</sub>@PFOTES-CV NPs is described in Fig. S17. The holder containing the test filter was reversely installed to allow clean air to enter. The face velocity of the air was adjusted to a range of 3–17 cm/s using the mass flow controller, and the concentration

of debris was measured using a condensation particle counter (model 3010, TSI Inc.). The equilibrium water contact angle of the TiO<sub>2</sub>@PFOTES-CV deposited filter was examined using a contact angle meter (CA-X, Kyowa Interface Science, Saitama, Japan) in static mode with a deionized water droplet (5 μL). The water contact angle was measured at five different locations on the surface of the test filter, and images were captured and analyzed. To confirm the stability of the TiO<sub>2</sub>@PFOTES-CV nanostructure on the antimicrobial air filters against water, 3 mL deionized water were dropped continuously on the surface of the TiO<sub>2</sub>@PFOTES-CV-based antimicrobial air filter to determine effusion of TiO<sub>2</sub>@PFOTES-CV particles. The test filter was tilted at an angle of 30°.



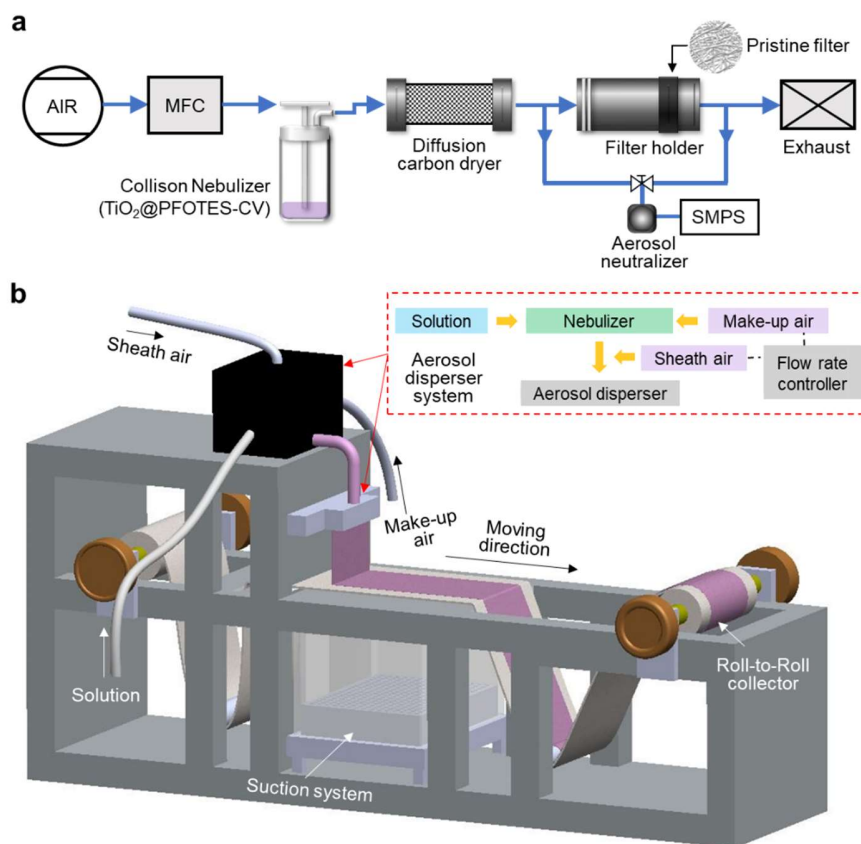
**Figure S1.** XPS spectra of Control,  $\text{TiO}_2$  and  $\text{TiO}_2$ @PFOTES-CV coated air filter. (a) Survey of control,  $\text{TiO}_2$  and  $\text{TiO}_2$ @PFOTES-CV coated filter. (b) Ti2p and O1s (inset image) scan of  $\text{TiO}_2$  and  $\text{TiO}_2$ @PFOTES-CV coated filter. (c) C1s scan of  $\text{TiO}_2$  and  $\text{TiO}_2$ @PFOTES-CV coated filter. Inset, C1s spectra contribution of  $\text{TiO}_2$ @PFOTES-CV. (d) F1s, (e) Si2p, and (f) N1s scan of  $\text{TiO}_2$ @PFOTES-CV coated filter. (g) Schematic of the  $\text{TiO}_2$  functionalization mechanisms of PFOTES by the silanization reaction.

Figure S1a presents the XPS survey data of each sample. As shown in Figs. S1b and c, the chemical bonding of Ti and O changed after PFOTES-CV modification; the binding energy of Ti2p varied from 458.51 to 458.74 eV, and that of O1s varied from 529.76 to 529.98 eV. In addition, contributions of C-F and C-Si-O (291.42 and 288.38 eV) were easily identified in the curve.<sup>2</sup> F1s and Si2p peaks were also observed in the  $\text{TiO}_2$ @PFOTES-CV-coated air filter, indicating the presence of  $\text{TiO}_2$  NPs with PFOTES

(Figs. S1d and e). These XPS results show a possibility that the triethoxy-silane group of PFOTES could be covalently bonded to the surface of TiO<sub>2</sub> NPs.<sup>3</sup> Hydrolysis of PFOTES produces the –Si–OH functional group, and a condensation reaction could occur between the –Si–OH and hydrophilic –OH functional groups in TiO<sub>2</sub>. So, the –OH functional groups in TiO<sub>2</sub> surface were modified with a long-chain alkyl group from PFOTES (Fig. S1g).<sup>4</sup>

A small peak in the N1s region was also present, indicating the presence of CV with TiO<sub>2</sub>@PFOTES NPs (Fig. S1f); therefore, CV was deposited on the TiO<sub>2</sub>@PFOTES NPs<sup>5,6</sup> and permeated through the interstitial spaces.<sup>7,8</sup> In addition, cationic CV may electrostatically bond with the anionic titanate of TiO<sub>2</sub>@PFOTES.





**Figure S2.** (a) Schematic representation of the aerosol deposition process for the preparing of VLA antimicrobial air filters in this study. (b) A methodological scheme is feasible for large-scale implementation.

The aerosol deposition method is simple and robust, and divided into two steps: (i) aerosol generation and (ii) aerosol deposition. The first step is the spraying of TiO<sub>2</sub>@PFOTES-CV solution into air by the interaction of capillary force and air pressure. Then, the generated nanosized aerosol particles are physically attached to the filter fiber. The main adhesive force is the van der Waals force. Also, we demonstrated the feasibility of continuous high-throughput aerosol-based coating methods for large-scale fabrication of antimicrobial air filters (Fig. S2).<sup>9</sup> This system enables uniform deposition of nanosized functional particles on pristine filter media and covers a filter area of 4,500 mm<sup>2</sup> using the roll-to-roll collector.

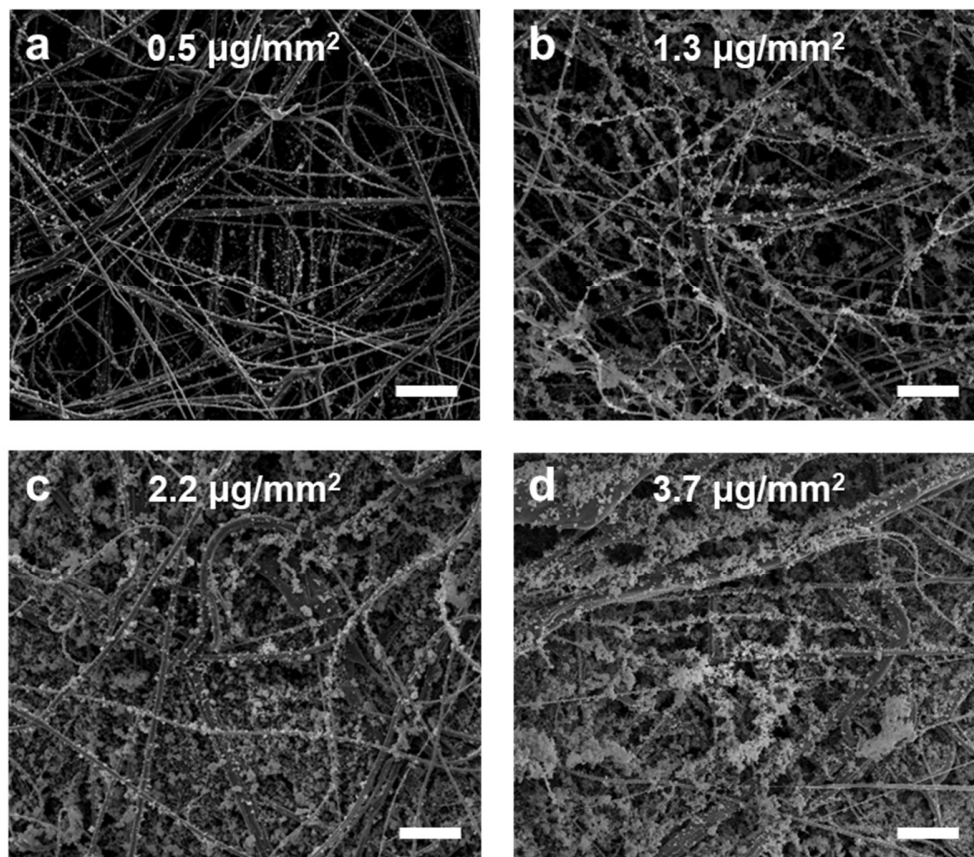


**Figure S3.** Scanning electron microscopy images of VLA antimicrobial filters, with  $\text{TiO}_2\text{@PFOTES-CV}$  deposition rates of (a) 0.5, (b) 1.3, (c) 2.2, and (d) 3.7  $\mu\text{g}/\text{mm}^2$ . Scale bars indicate 50  $\mu\text{m}$ .

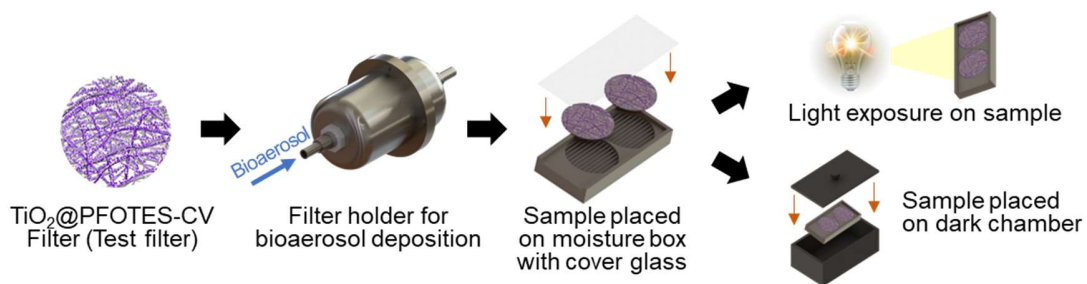


**Figure S4.** Schematic representations of the procedure for VLA antimicrobial effects verification.

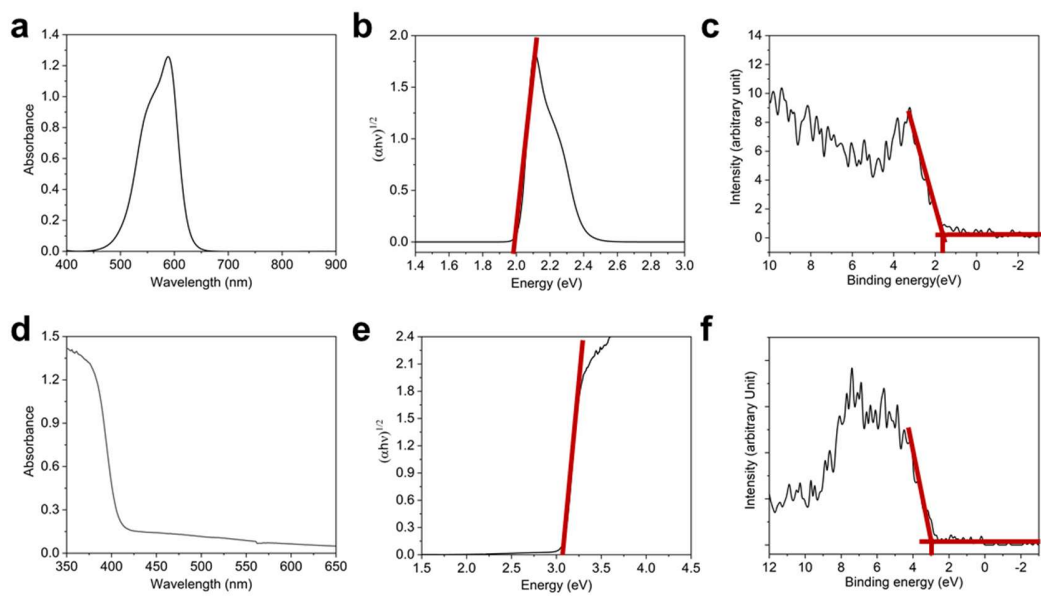


**Figure S5.** (a) UV-Vis absorbance spectrum, (b) band gap, and (c) homo band of phase-pure CV. (d) UV-Vis absorbance spectrum, (e) band gap, and (f) valance band of phase-pure TiO<sub>2</sub>.

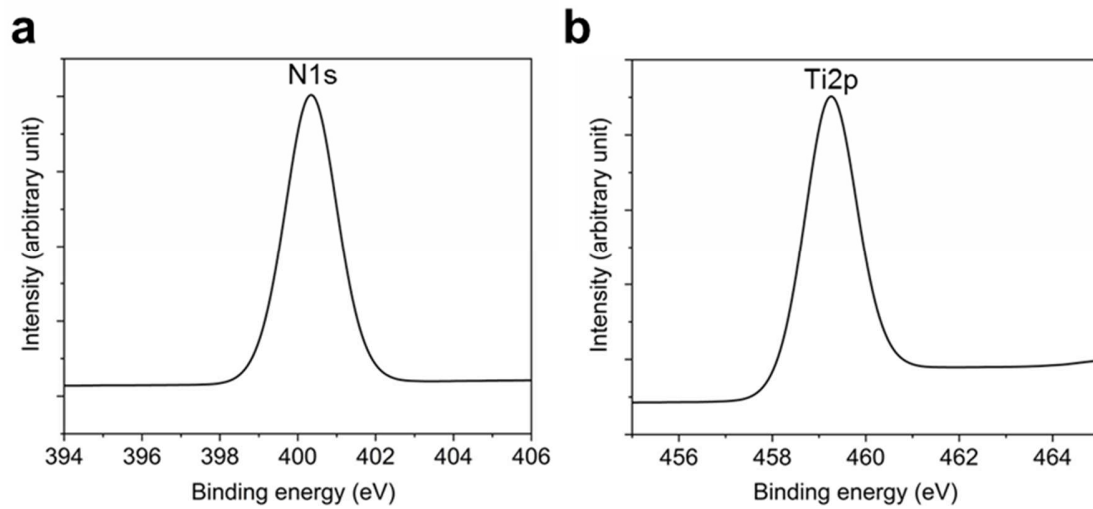


**Figure S6.** (a) N1s and (b) Ti2P spectra of CV and TiO<sub>2</sub>.

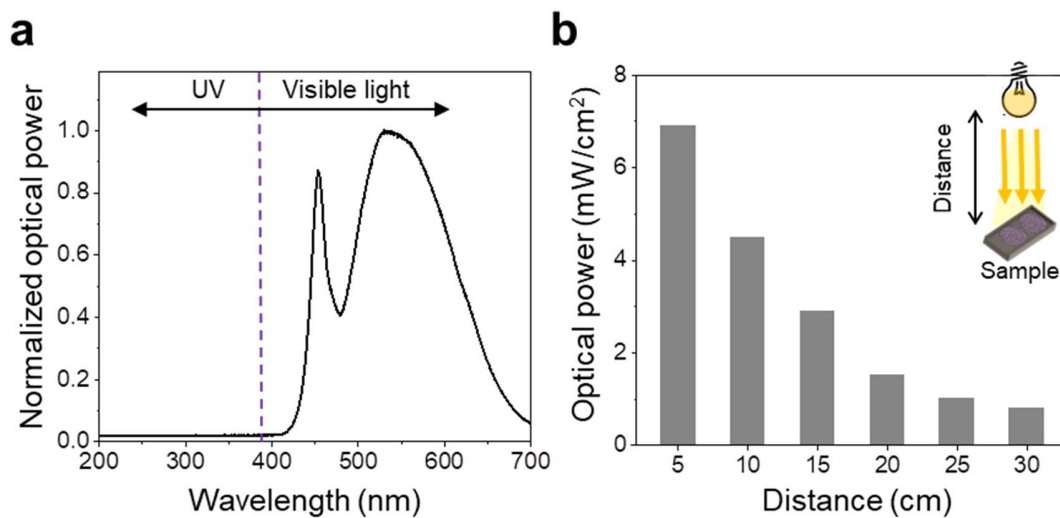


**Figure S7.** Light source information. (a) The spectrum measurement results obtained using a spectrometer (USB2000+; Ocean Optics, Dunelin, FL, USA) and (b) the optical power depend on the distance between the light source and the sample measured by a power meter and a photodiode power sensor (PM200; S120C; Thorlabs Inc.).

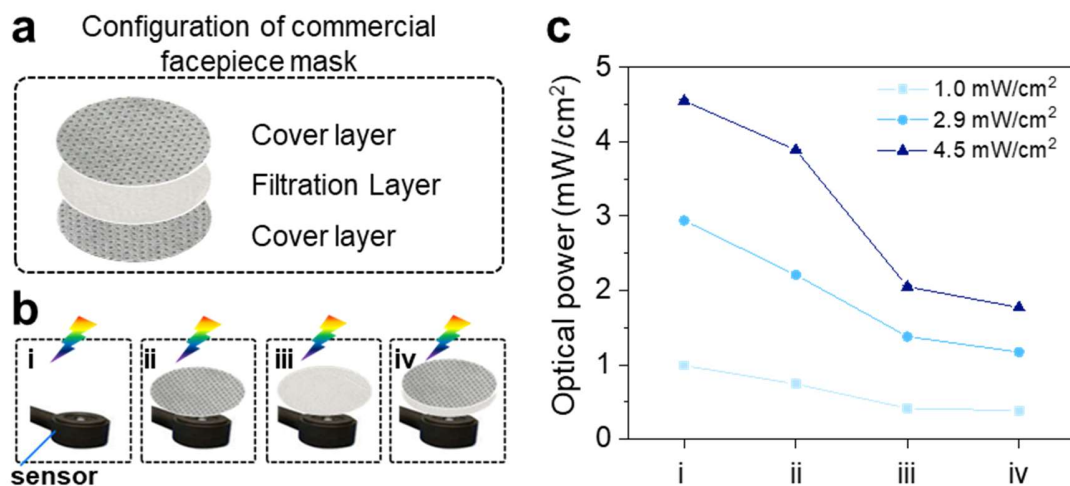


**Figure S8.** Light intensity according to the filter layer configuration. (a) Configuration of a prepared commercial facepiece mask. (b) Test setup for light intensity according to the filter layer configuration. (c) Change of light intensity change according to the filter layer configuration.

The filtration layer of the commercial air filter inevitably has an outer cover layer, which has a low packing density, to protect the filtration layer (Fig. S8a). Although the light intensity decreased ~25, ~25, and ~15% as light passed through the cover layer at light intensity of 1.0, 2.9, and 4.5 mW/cm<sup>2</sup>, respectively (Fig. S8c), sufficient light to induce photochemical reaction reaches the TiO<sub>2</sub>@PFOTES-CV nanostructures on the filter layer. But, the reduction of light intensity is still an important issue because it influences the VLA antimicrobial performance of TiO<sub>2</sub>@PFOTES-CV NPs, which are mostly coated on the internal filtration layer. In addition, this could have a significant impact on the realization of photochemical inactivation, especially under low level of light. Combining transparent air filters and visible-light-activated antimicrobial materials, however, would overcome the deterioration of light intensity.

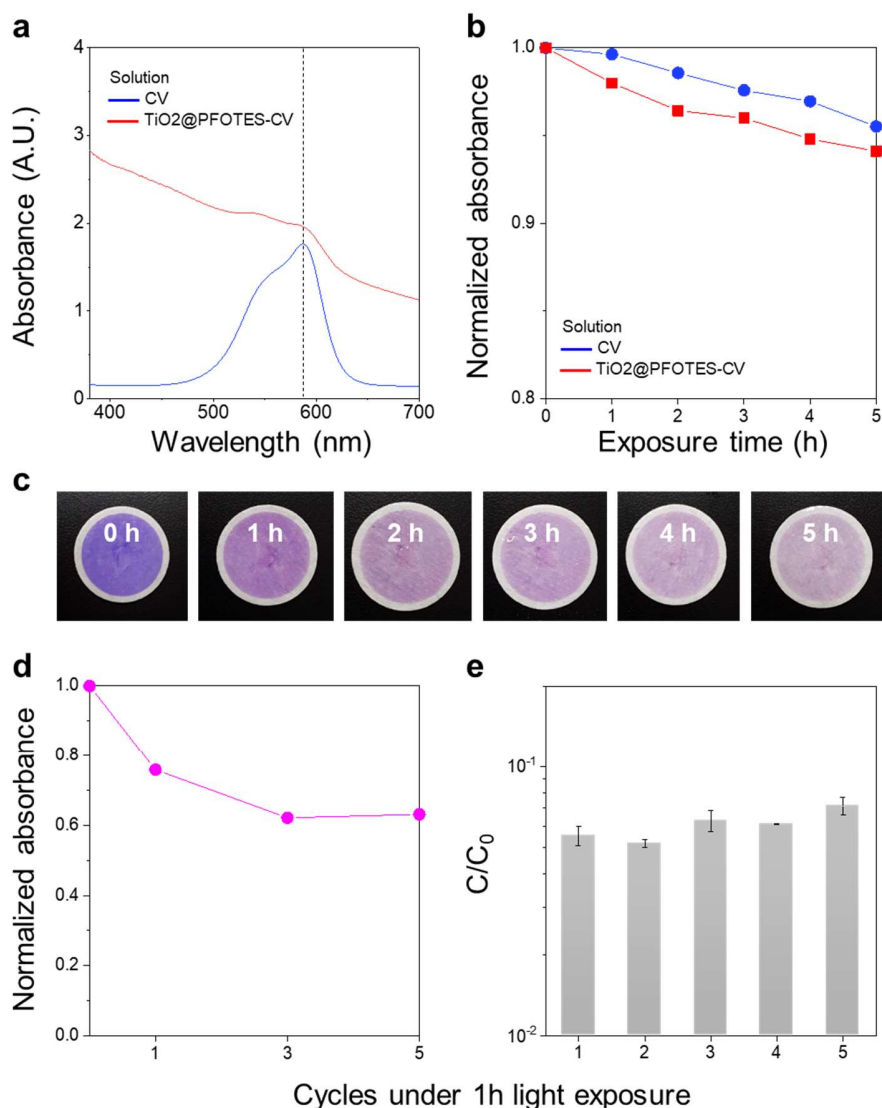


**Figure S9.** Photostability of the TiO<sub>2</sub>@PFOTES-CV filter under light exposure. (a) UV-Vis absorbance spectra of CV and TiO<sub>2</sub>@PFOTES-CV solution. (b) Normalized absorbance at the CV absorbance peak of CV and TiO<sub>2</sub>@PFOTES-CV solution according to light exposure duration. The solutions were illuminated with a visible-light source emitting an average optical power of 2.9 mW/cm<sup>2</sup> (15 cm from the solution). (c) Digital images of TiO<sub>2</sub>@PFOTES-CV air filter according to light exposure duration. (d) Normalized absorbance at the CV absorbance peak of TiO<sub>2</sub>@PFOTES-CV-coated air filter solution according to light exposure duration. (e) Long-term antimicrobial performance of a TiO<sub>2</sub>@PFOTES-CV-coated air filter.



Figure S9a shows the UV-Vis absorbance spectra (400–700 nm) of TiO<sub>2</sub>@PFOTES-CV and CV solution. The solutions were illuminated with a visible-light source emitting an average optical power of 2.9 mW/cm<sup>2</sup> (15 cm from the solution). The photodegradation rate of CV solution was 5% over 5 h. Over the same period, TiO<sub>2</sub>@PFOTES-CV solution also showed a ~6% photodegradation rate in the CV peak, indicating that the ROS generated by TiO<sub>2</sub> did not significant role in degradation of CV (Fig. S9b). However, during the same period, the TiO<sub>2</sub>@PFOTES-CV coated filter shows a distinct change in color, indicating a photodegradation of CV (Fig. S9c). Normalized absorbance at the CV absorbance maxima was reduced to ~38% after just 3 h of light exposure (Fig. S9d). These results indicate that the structure formed by TiO<sub>2</sub>@PFOTES-CV NPs accelerates the visible-light activated reaction.

To evaluate the robustness of the antimicrobial performance of TiO<sub>2</sub>@PFOTES-CV, we performed a cyclic contact-killing test. Each cycle consisted of a visible-light-activated antimicrobial experiment with 1 h of light exposure and cleaning of the test filter with water. Bacterial suspension (1 mL) was spotted on the surface of a TiO<sub>2</sub>@PFOTES-CV air filter and exposed to visible light for 1 h. The bacterial suspension was decanted and subjected to plate count. The number of bacteria decreased slightly from 1.17 to 1.06 log during the test (Fig. S9e). Although changes in filter color were observed and light-induced degradation of TiO<sub>2</sub>@CV occurred, the antimicrobial performance of TiO<sub>2</sub>@PFOTES-CV remained constant over 5.306 h, i.e., the average daily duration of mask use.<sup>10</sup>

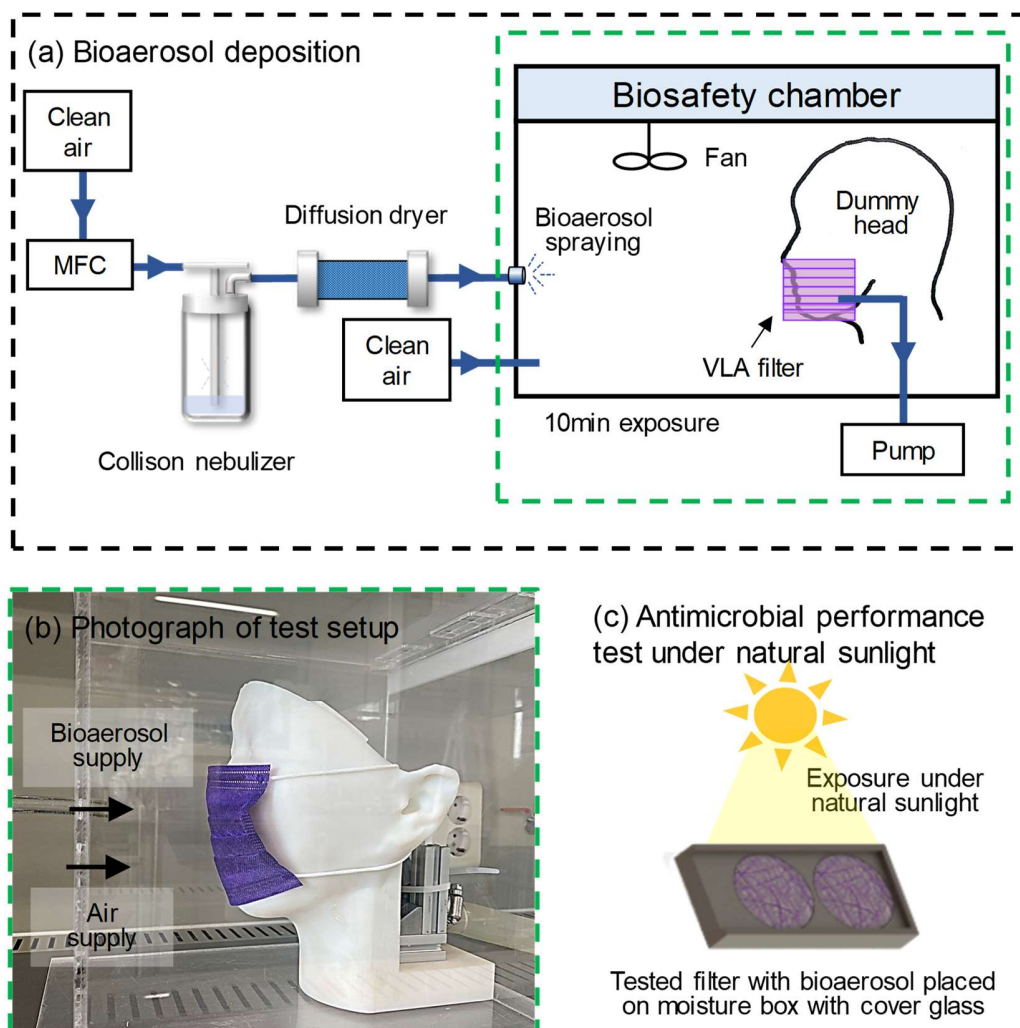


**Figure S10.** Schematic of the antimicrobial performance evaluation experimental setup of  $\text{TiO}_2\text{@PFOTES-CV}$  filter under real sunlight condition. (a) Bioaerosol deposition process and (b) photograph of test setup marked with a dashed green box in Fig. S10a. Clean air was injected a 24 jet-Collison nebulizer for generation of *S. epidermidis* bioaerosols at a flowrate of 20.0 L/min. Seal the  $\text{TiO}_2\text{@PFOTES-CV}$  filter on the dummy head. The generated bioaerosols deposited onto the  $\text{TiO}_2\text{@PFOTES-CV}$  filter for 10 min under the standard inhalation airflow rate of 30.0 L/min suggested by test protocol of 42 CFR part 84 (APPROVAL OF RESPIRATORY PROTECTIVE DEVICES).<sup>[S2]</sup> Subsequently, the tested filter were exposed to natural sunlight. (c) Schematic diagram of the experimental setup for antimicrobial performance of  $\text{TiO}_2\text{@PFOTES-CV}$  filter under natural sunlight.

The tested control and TiO<sub>2</sub>@PFOTES-CV filter with bioaerosols were placed on a moisture box to maintain humidity and covered with a sterile glass slide to maintain proper contact between the surface of the test filter and the bacteria. Subsequently, the filters were exposed to natural sunlight. Following light exposure, the samples were placed in 15 mL ( $V_{\text{extraction, filter}}$ ) phosphate-buffered saline (PBS) containing 0.01% Tween 80 and vortexed for 5 min to transfer the bacterial particles from the filter to the PBS solution. The resulting bacterial suspension from the test filters was serially diluted onto a nutrient agar plate (0.3% beef extract and 0.5% peptone; Becton Dickinson) and incubated at 37°C for 24 h. Bacterial colony forming units (CFUs) were counted after incubation.

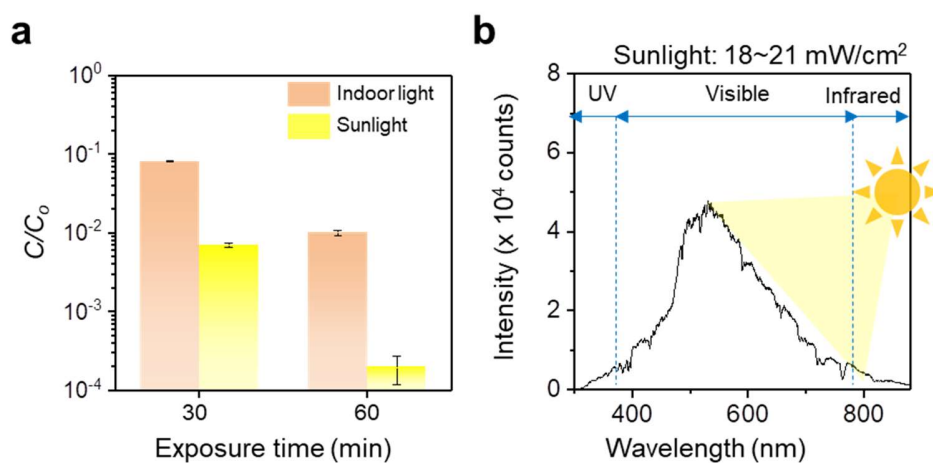


**Figure S11.** Antimicrobial performance of VLA antimicrobial air filter under natural sunlight condition. (a) Bactericidal activity of the TiO<sub>2</sub>@PFOTES-CV filters against *S. epidermidis* under indoor artificial light (6.9 mW/cm<sup>2</sup>) and natural sunlight irradiation conditions. C<sub>0</sub> and C are the number concentrations obtained from the control and TiO<sub>2</sub>@PFOTES-CV filter, respectively. (b) Spectrum of natural sunlight. The optical power of natural sunlight is 18-21 mW/cm<sup>2</sup> measured by a power meter and a photodiode power sensor. Natural sunlight contains a broad spectrum compared indoor artificial light, all the way from ultraviolet to near-infrared light.

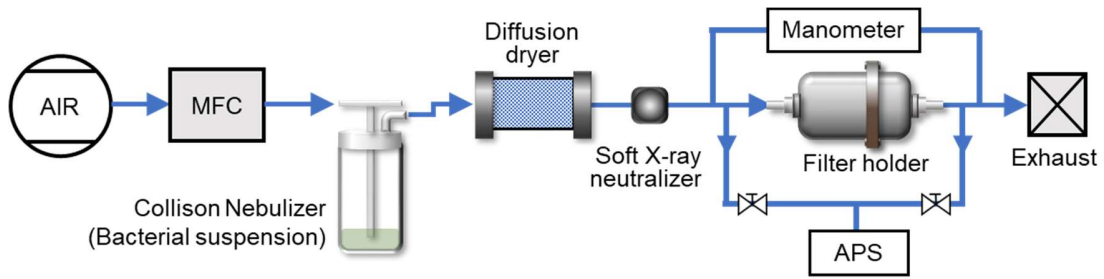


**Figure S12.** Schematic diagram of the filtration performance test using bioaerosols.

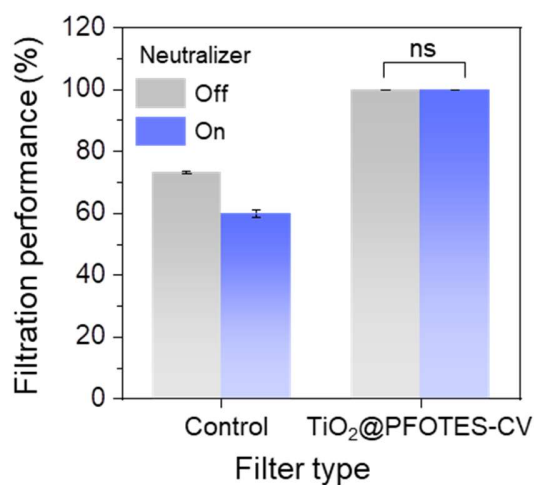


**Figure S13.** Filtration performance of TiO<sub>2</sub>@PFOTES-CV filters according to the aerosol neutralizer use. Filtration performance of control and TiO<sub>2</sub>@PFOTES-CV filters against *S. epidermidis* bioaerosols. (ns: no significant difference,  $p > 0.05$ )

The filtration performance of the control filter decreased after aerosol neutralization, but that of TiO<sub>2</sub>@PFOTES-CV did not vary significantly irrespective of aerosol neutralization. This can be explained by the filtration mechanisms of TiO<sub>2</sub>@PFOTES-CV filters. The inertial impaction of the TiO<sub>2</sub>@PFOTES-CV-coated air filter is enhanced by abrupt changes in air streamline by the 3D structure of the TiO<sub>2</sub>@PFOTES-CV NPs. Therefore, the 3D structure of the TiO<sub>2</sub>@PFOTES-CV NPs enhanced the probability of collision with bacteria in the vicinity.

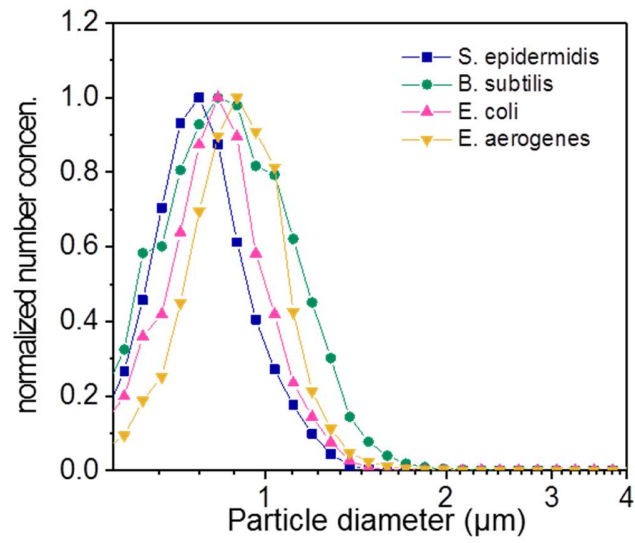


**Figure S14.** Particle size distribution of *Staphylococcus epidermidis*, *Bacillus subtilis*, *Escherichia coli*, and *Enterobacter aerogenes* bioaerosols measured using an aerodynamic particle sizer.

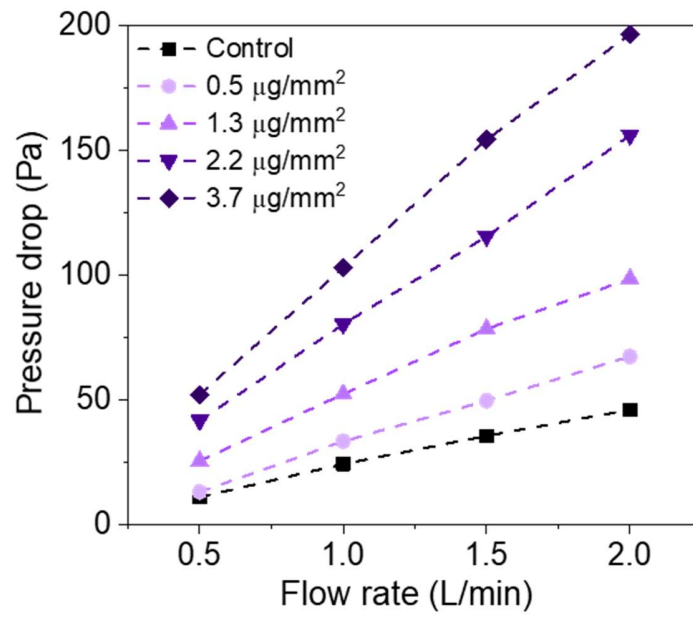


**Figure S15.** Pressure drop versus flow rate of TiO<sub>2</sub>@PFOTES-CV-based air filters prepared at different coating times.



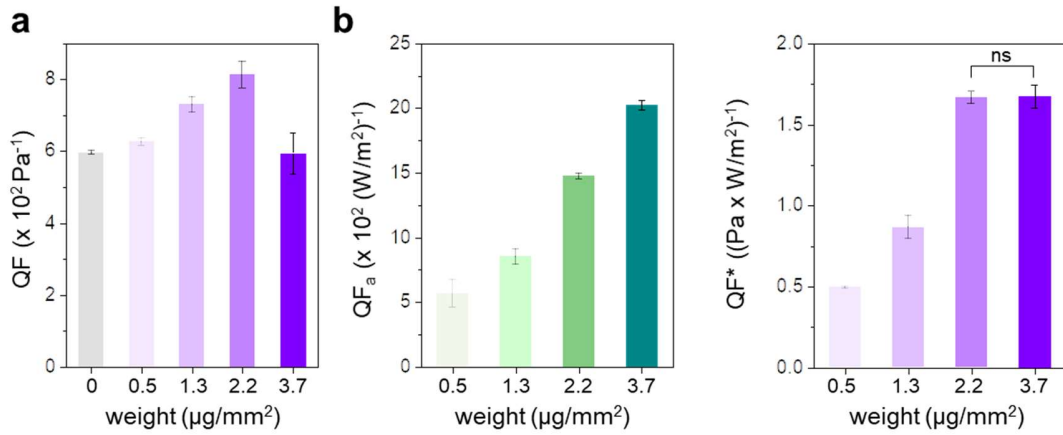


**Figure S16.** (a) Quality factor for (a) bacteria capture performance (QF) and (b) light-induced antimicrobial performance (QF<sub>a</sub>). (C) QF\* of TiO<sub>2</sub>@PFOTES-CV-based air filters according to coating time. (ns: no significant difference,  $p > 0.05$ )

In general, to determine if an air filter is efficient, the QF is calculated using the following formula:<sup>11,12</sup>

$$QF = - \frac{\ln(1-\eta)}{\Delta P} \quad (6)$$

According to this formula, a higher QF indicates higher filtration ability per unit mechanical energy input. The QF of the TiO<sub>2</sub>@PFOTES-CV filter dramatically increased when the TiO<sub>2</sub>@PFOTES-CV concentration increased from 1.3 to 2.2 µg/cm<sup>2</sup> (Fig. S16a). However, at 0.5 µg/cm<sup>2</sup> deposition, the QF was similar to that of the control due to insufficient 3D structure formation on the filter fiber. In addition, the QF value at a deposition weight > 2.2 µg/cm<sup>2</sup> decreased, because the pressure drop increased while the filtration performance had peaked. Thus, a concentration of 2.2 µg/cm<sup>2</sup> is optimal in terms of the pressure drop and filtration efficiency.

However, although the QF value is useful for analyzing the energy-efficiency with respect to particle removal, it is insufficient to evaluate the antimicrobial performance. Therefore, we propose a QF<sub>a</sub> for light-induced antimicrobial performance based on the principle of QF. We focus on the evaluation of the antimicrobial performance and energy cost of the light source. If each filter layer has a constant antimicrobial activity per unit reaction time,  $\beta$ , the number of inactivated bacteria during  $\delta t$  can be expressed as,

$$\delta C = -\beta C \delta t. \quad (7)$$

Integrating Eq. (9) gives the particle penetration of the filter, as follows:

$$-\beta t = \ln \left( \frac{C_{\text{survival}}}{C_{\text{initial}}} \right), \quad (8)$$

$$e^{-\beta t} = \frac{C_{\text{survival}}}{C_{\text{initial}}} = S, \quad (9)$$

$$\beta = \frac{\ln(1/S)}{t}. \quad (10)$$

where  $t$  is reaction time and  $S$  is the survival efficiency of capture bioaerosols.  $QF_a$  is the ratio of  $\beta$  to the light power per unit reaction time,  $\Delta E/t$ .

$$QF_a = \frac{\beta t}{\Delta E} = \frac{\ln(1/S)}{\Delta E}, \quad (11)$$

According to this formula, a large  $QF^*$  indicates better antimicrobial performance per unit light power. The  $QF_a$  of the  $\text{TiO}_2@\text{PFOTES-CV}$  filter increased exponentially with increasing  $\text{TiO}_2@\text{PFOTES-CV}$  concentration (Fig. S16b). In order to determine the concentration that optimizes pressure drop (capture of bacteria) and antimicrobial performance. Therefore, we propose a modified QF ( $QF^*$ ), given by

$$QF^* = QF \times QF_a. \quad (12)$$

The  $QF^*$  of the  $\text{TiO}_2@\text{PFOTES-CV}$  filter dramatically increased when the  $\text{TiO}_2@\text{PFOTES-CV}$  concentration increased from 1.3 to 2.2  $\mu\text{g}/\text{cm}^2$  (Fig. S16c). The  $QF^*$  value at a deposition weight  $> 2.2 \mu\text{g}/\text{cm}^2$  showed no significant difference, because antimicrobial performance continuously increased but the efficient of bacteria filtration performance is already saturated. Thus, a concentration of 2.2  $\mu\text{g}/\text{cm}^2$  is optimal in terms of filtration and antimicrobial performance.

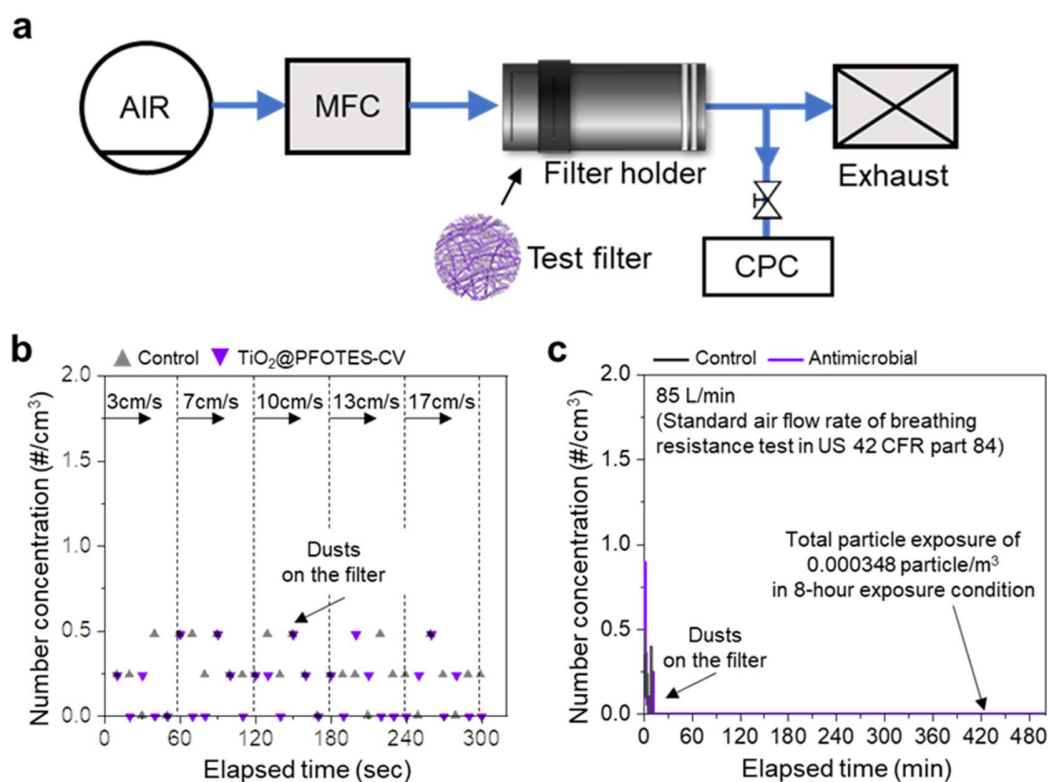


**Figure S17.** TiO<sub>2</sub>@PFOTES-CV nanostructure adhesion stability test. (a) Schematic of the TiO<sub>2</sub>@PFOTES-CV nanostructure adhesion stability test against airflow. (b) Stability of deposited TiO<sub>2</sub>@PFOTES-CV nanostructures under various air face velocity conditions. (c) Long-term stability of deposited TiO<sub>2</sub>@PFOTES-CV nanostructures under 85 L/min air flow, simulating breathing at a high work rate

The stability test showed that TiO<sub>2</sub>@PFOTES-CV NPs hardly come off the filter fiber. Thus, we believe that the visible-light-activated antimicrobial air filter will have a minor effect on human health.

**Table S1.** Comparison of adhesive, gravitational, and air drag forces on spherical particles of standard density.

Diameter, $d$ , (nm)	Force (N)		
	Adhesion*	Gravity	Drag force by air** (at 5 cm/s)
10	$9.14 \times 10^{-9}$	$5 \times 10^{-21}$	$8.6 \times 10^{-14}$
100	$9.14 \times 10^{-8}$	$5 \times 10^{-18}$	$8.6 \times 10^{-12}$
1000	$9.14 \times 10^{-7}$	$5 \times 10^{-15}$	$8.6 \times 10^{-10}$

\*Adhesion force<sup>13</sup> =  $0.063d[1+0.009(\text{Humidity}\%)]$  for 50% humidity

\*\*Drag force<sup>13</sup> =  $(\text{coefficient of drag})(\pi/8)(\text{density of air})(\text{air velocity})^2d^2$  for density of air at 20°C and 5 cm/s of air velocity

Particle adhesive forces are proportional to particle diameter,  $d$ , while removal forces are proportional to  $d^3$  for gravitational, vibrational, and centrifugal forces and  $d^2$  for drag forces by air currents. This relationship shows that as the particle size decreases, it becomes easier to hold the particle stably on the surface. Especially, the adhesion of nanosize particles and surfaces is much greater than other forces on such particles. Therefore, TiO<sub>2</sub>@PFOTES-CV nanosized particles are not likely to be detached by common forces.

## References

- (1) Li, P.; Li, J.; Feng, X.; Li, J.; Hao, Y.; Zhang, J.; Wang, H.; Yin, A.; Zhou, J.; Ma, X.; Wang, B. Metal-Organic Frameworks with Photocatalytic Bactericidal Activity for Integrated Air Cleaning. *Nat. Commun.* **2019**, *10* (1), 1–10.
- (2) Gonbeau, D.; Guimon, C.; Pfister-Guillouzo, G.; Levasseur, A.; Meunier, G.; Dormoy, R. XPS Study of Thin Films of Titanium Oxysulfides. *Surf. Sci.* **1991**.
- (3) Barlow, S. M.; Raval, R. Complex Organic Molecules at Metal Surfaces: Bonding, Organisation and Chirality. *Surf. Sci. Rep.* **2003**, *50* (6–8), 201–341.
- (4) Zhang, H.; Li, Y.; Lu, Z.; Chen, L.; Huang, L.; Fan, M. A Robust Superhydrophobic TiO<sub>2</sub> NPs Coated Cellulose Sponge for Highly Efficient Oil-Water Separation. *Sci. Rep.* **2017**, *7* (1), 3–10.
- (5) Luo, X.; Kim, J. H.; Ahn, J. Y.; Lee, D.; Kim, J. M.; Lee, D. G.; Kim, S. H. Electro spraying-Assisted Rapid Dye Molecule Uptake on the Surfaces of TiO<sub>2</sub> Nanoparticles for Speeding up Dye-Sensitized Solar Cell Fabrication. *Sol. Energy Mater. Sol. Cells* **2016**, *144*, 411–417.
- (6) Hwang, G. B.; Patir, A.; Allan, E.; Nair, S. P.; Parkin, I. P. Superhydrophobic and White Light-Activated Bactericidal Surface through a Simple Coating. *ACS Appl. Mater. Interfaces* **2017**, *9* (34), 29002–29009.
- (7) Elakkiya, S.; Arthanareeswaran, G.; Ismail, A. F.; Das, D. B.; Suganya, R. Polyaniline Coated Sulfonated TiO<sub>2</sub> Nanoparticles for Effective Application in Proton Conductive Polymer Membrane Fuel Cell. *Eur. Polym. J.* **2019**, *112*, 696–703.
- (8) Mashkoo, F.; Nasar, A.; Inamuddin; Asiri, A. M. Exploring the Reusability of Synthetically Contaminated Wastewater Containing Crystal Violet Dye Using Tectona Grandis Sawdust as a Very Low-Cost Adsorbent. *Sci. Rep.* **2018**, *8* (1), 1–16.
- (9) Kang, J. S.; Kim, H.; Choi, J.; Yi, H.; Seo, S. C.; Bae, G. N.; Jung, J. H. Antimicrobial Air Filter Fabrication Using a Continuous High-Throughput Aerosol-Based Process. *Aerosol Air Qual. Res.* **2016**, *16* (8), 2059–2066.
- (10) Chao, F. Adolescents' Face Mask Usage and Contact Transmission in Novel Coronavirus. **2020**, *9*, 36–39.
- (11) Singh, V. K.; Ravi, S. K.; Sun, W.; Tan, S. C. Transparent Nanofibrous Mesh Self-Assembled from Molecular LEGOs for High Efficiency Air Filtration with New Functionalities. *Small* **2017**.
- (12) Liu, C.; Hsu, P. C.; Lee, H. W.; Ye, M.; Zheng, G.; Liu, N.; Li, W.; Cui, Y. Transparent Air Filter for High-Efficiency PM 2.5 Capture. *Nat. Commun.* **2015**, *6* (1), 1–9.
- (13) Hinds, W. C. *Aerosol Technology: Properties, Behaviour, and Measurement of Airborne Particles*; John Wiley & Sons, 1982.